Modeling of Turbulent Flowfields Through a Cascade of Airfoils at Stall Conditions

C. Hah*
General Electric Company, Schenectady, New York

A numerical method of predicting the properties of turbulent flows through a cascade of airfoils at stall conditions has been developed and appraised. The numerical scheme is based on the fully conservative control volume representation of governing Navier-Stokes equations and solves the governing equations in elliptic form. Two different turbulence closure schemes (two-equation model and an algebraic Reynolds stress model) are used and compared for the effects of the streamline curvature. Comparisons with the available experimental data show that the present method predicts complex turbulent flows through a cascade of airfoils at stall conditions with accuracy satisfactory for engineering purposes.

Nomenclature

b = blade chord
$C_S, C_1, C_\epsilon, C_{\epsilon 1}, C_{\epsilon 2}, \gamma, D_6$ = constants in turbulence closure models
C = mean temperature
c = fluctuating temperature
c_d, c_l = section drag and lift coefficients, respectively
c_p = specific heat
C_p = static pressure coefficient, $= (P - P_1) \div \frac{1}{2}\rho_1 U_1^2$
F_a, F_u = axial and tangential components of acting force on blades, respectively
g = tangential spacing between blades
k = turbulence kinetic energy
k_c = thermal conductivity
P = $-\overline{u_i u_j} U_{i,j}$
p = static pressure
p' = fluctuating component of static pressure
R = gas constant
S = pressure coefficient, $= (1 - C_p)$
U, u = axial components of mean and fluctuating velocity
V, v = tangential components of mean and fluctuating velocity
β = angle between flow direction and a perpendicular to the cascade axis
δ_{ij} = Kronecker delta
ϵ = rate of turbulent kinetic energy dissipation
θ = flow turning angle
ν = kinematic viscosity
ρ = density
σ = solidity, $= b/g$
τ_w = wall shear stress

Subscripts

a = component in axial direction
m = referred to vector-mean velocity, $= W_m$
u = component in tangential direction
$1,2$ = upstream and downstream of blade row, respectively

Superscripts

$(\bar{})$ = average value

Introduction

THE accurate prediction of the turbulent flowfields inside a cascade of airfoils over a wide range of flow conditions is very important for both scientific and engineering purposes. Although significant progress has been made recently in the viscous flow solution of the problem (see, e.g., Refs. 1-3), no attempts have been made to compare the predictions for the aerodynamic characteristics near or at stall conditions. Although reasonable agreement of the static pressure distribution on the blade surface indicates the usefulness of various numerical schemes, careful comparison of the velocity, wall shear stress, and wake mixing should be made for the reliable estimation of the aerodynamic performance of the stage.

The present study is aimed at developing and appraising a numerical model to predict turbulent flowfields through a cascade of airfoils at stall conditions. In general, the flowfield around a cascade of airfoils could be characterized as pressure-dominated flow when no significant flow separation is developed.[4] At stall conditions, the amount of separated flowfields is very sensitive to the physical diffusion of the flow and overall aerodynamic characteristics of the stage (blade surface static pressure distribution, lift/drag coefficient, and turning angle, etc.) are also significantly affected. Therefore, the problems of numerical diffusion and proper turbulence closure modeling should be examined carefully.

The numerical scheme employed for the present study is based on the fully conservative control volume, and the governing Navier-Stokes equations are solved on generalized nonorthogonal curvilinear coordinates. Body-fitted coordinates are numerically generated to represent the geometry of the airfoil, and coordinate stretching is performed near the airfoil. To reduce numerical diffusion with affordable computational grids, the quadratic upwind interpolation scheme of Leonard[5] has been properly modified and used to discretize the convection terms of the governing equations.

Various studies[6-8] have indicated that turbulent flows with large amounts of flow separation are strongly affected by the streamline curvature, and the effects of the streamline curvature should be properly represented in the closure scheme

Presented as Paper 83-1743 at the AIAA 16th Fluid and Plasma Dynamics Conference, Danvers, Mass., July 12-14, 1983; revision received Oct. 15, 1983; revision received Dec. 10, 1984.

*Fluid Mechanics Engineer, Corporate Research and Development. Member AIAA.

for accurate prediction. For the present study, two different turbulence closure schemes (the conventional two-equation model and an algebraic Reynolds stress model) are tested and the results are compared with the experimental data.

The governing equations and turbulence closure schemes are described in the next section. The numerical procedure and adopted grids are discussed in the following section, and the numerical results are then compared with the experimental data. The conclusions drawn from this study are given in the last section.

Governing Equations and Turbulence Closure Modeling

Various conservation equations for the viscous flow considered are as follows:

Mass:

$$\frac{1}{\rho}\frac{\mathrm{D}\rho}{\mathrm{D}t}+U_{i,i}=0 \tag{1}$$

Momentum:

$$\rho\frac{\mathrm{D}U_i}{\mathrm{D}t}=\rho F_i-\frac{\partial p}{\partial x_i}+\frac{\partial}{\partial x_j}\left(\mu\frac{\partial U_i}{\partial x_j}-\rho\overline{u_iu_j}\right) \tag{2}$$

Energy:

$$c_p\frac{\mathrm{D}C}{\mathrm{D}t}-\frac{\beta C}{\rho}\frac{\mathrm{D}p}{\mathrm{D}t}=\theta+\frac{1}{\rho}\frac{\partial}{\partial x_i}\left(k_c\frac{\partial C}{\partial x_i}-\overline{u_ic}\right) \tag{3}$$

Gas state:

$$p=\rho RC \tag{4}$$

where U_i is the mean velocity, u_i the fluctuating velocity, C the mean temperature, c the fluctuating temperature, θ the dissipation due to viscosity, β the coefficient of thermal expansion, F_i the additional body force, and R the gas constant.

To get closure of the above system of equations, the turbulent diffusion terms should be described with proper means. For the present study, the following two different turbulence closure schemes are used:

$$U_i\frac{\partial k}{\partial x_i}=\frac{\partial}{\partial x_i}\left(\frac{\nu_{\mathrm{eff}}}{\sigma_k}\frac{\partial k}{\partial x_i}\right)+P-\epsilon \tag{5}$$

$$U_i\frac{\partial \epsilon}{\partial x_i}=\frac{\partial}{\partial x_i}\left(\frac{\nu_{\mathrm{eff}}}{\sigma_\epsilon}\frac{\partial \epsilon}{\partial x_i}\right)+S-C_{\epsilon 2}\frac{\epsilon^2}{k} \tag{6}$$

where

$$\nu_{\mathrm{eff}}=C_\mu k^2/\epsilon, \qquad k=\tfrac{1}{2}\delta_{ij}\overline{u_iu_j}=\nu_{\mathrm{eff}}(U_{i,j}+U_{j,i})-\tfrac{2}{3}k\delta_{ij}$$

and P and S are source terms in the turbulence kinetic energy and energy dissipation equations.

$$P=\nu_{\mathrm{eff}}\left(\frac{\partial U_i}{\partial x_j}+\frac{\partial U_j}{\partial x_i}\right)\frac{\partial U_i}{\partial x_j} \tag{7}$$

$$S=C_{\epsilon 1}(\epsilon/k)P \tag{8}$$

Second Model

This model is based on the simplified Reynolds stress transport equation and the individual nonzero Reynolds stress components are estimated with the following algebraic relationship:

$$0=(1+C_1)(-\overline{u_ku_j}U_{i,k}-\overline{u_ku_i}U_{j,k})(1-\gamma)$$
$$-\tfrac{2}{3}\delta_{ij}(1-\gamma)-C_{\phi 1}(\epsilon/k)(\overline{u_iu_j}-\tfrac{2}{3}\delta_{ij}) \tag{9}$$

where γ and $C_{\phi 1}$ are constants in the modeling and C_1 is a variable that represents the collective effects of the convection and the diffusion terms in the exact transportation equations of the Reynolds stresses.

A detailed description of the above model has been reported previously in Ref. 9. To get the above algebraic relationship for Reynolds stresses, the net effect of convection and diffusion in the equation is assumed to be related to the transportation of the turbulence kinetic energy by

$$A_{ij}=(P_{ij}/P)(P-\epsilon) \tag{10}$$

where

$$P_{ij}=-\overline{u_ku_j}U_{i,k}-\overline{u_ku_i}U_{j,k} \tag{11}$$

$$P=-\overline{u_iu_j}U_{i,j} \tag{12}$$

With the second model, transport equations for the turbulence kinetic energy and energy dissipation rate are solved simultaneously along with the governing equations (1-4), and the algebraic equation (9) is used for stress terms. The same transport equations for the turbulence kinetic energy and energy dissipation rate are used for both models. However, the source term P in Eq. (5) is evaluated with Eq. (12), and S in Eq. (6) is replaced with the following form for the second model:

$$S=C_S(\epsilon^2/k^3)(\overline{u_iu_j}-\tfrac{2}{3}k\delta_{ij})(\overline{u_ju_i}-\tfrac{2}{3}k\delta_{ji})-C_R\overline{u_iu_j}U_{i,j} \tag{13}$$

where $C_S=1.8$ and $C_R=0.46$. The basic difference between the first and second models is how to estimate the value of individual stress terms with the given values of turbulence kinetic energy and energy dissipation rate. The first model uses isotropic effective eddy viscosity, while the second model solves algebraic equations with approximately represented effects of the convection and diffusion of Reynolds stresses. As is well known, the local turbulence structure as well as the mean velocity field are altered considerably due to the effect of streamline curvature. While the first model does not represent the streamline curvature effects properly,[6] the second model represents the gross curvature effects more adequately when the net effect of convection and diffusion is less important than the net effect of production and dissipation.[7] The overall effect of streamline curvature is to stabilize the flowfield and, consequently, to diminish the turbulent diffusion when the angular momentum increases with the radius of streamline curvature, and vice versa for the opposite case. This effect is represented in the turbulence kinetic energy equation through the production term P. For the flow with the streamline curvature, the extra strain rate can either increase or decrease the level of production depending on the curvature effect. With the source term [Eq. (13)] in the energy dissipation equation,

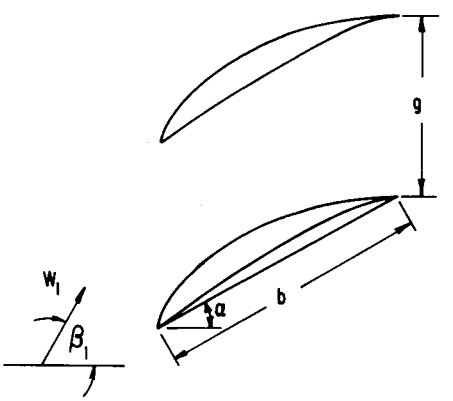

Fig. 1 Notations for the flow around the cascade of airfoils.

the level of energy dissipation rate is less directly related to the production of turbulence kinetic energy compared to the term [Eq. (8)] and the resulting length scale for turbulent diffusion ($1 \sim k^2/\epsilon$) is more closely related to the gross curvature effects. Although the dissipation equation (6) can be modified based on the Richardson number for the curvature effects,[10,11] the current problem involves multiple components of streamline curvature; this approach is not taken herein.

Numerical Scheme and Boundary Conditions

Numerical Algorithm

The governing conservation equations are solved using a fully conservative control volume approach along with turbulence closure equations. The various governing equations are expressed in the following general form for the convenience of the formulation:

$$(\rho U_i \phi^{n+1})_{,i} = (\Gamma \phi^{n+1}_{,i}) + S_\phi \tag{14}$$

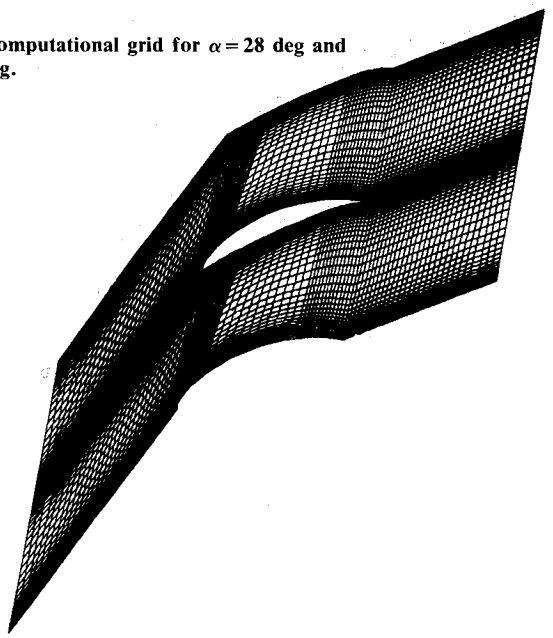

Fig. 2 Computational grid for $\alpha = 28$ deg and $\beta_1 = 60$ deg.

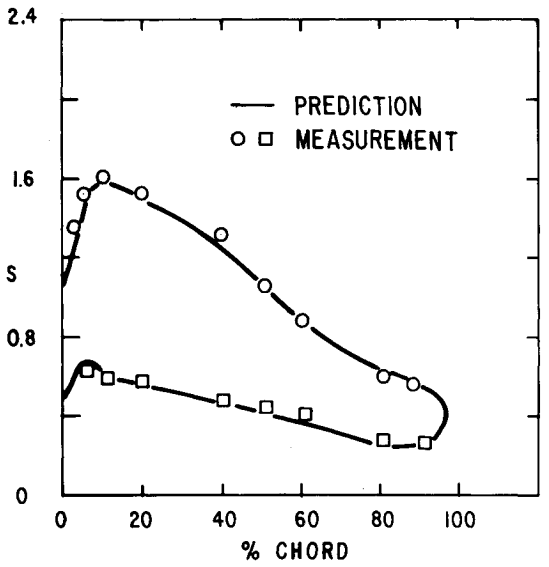

Fig. 3 Comparison of static pressure distribution for $\alpha = 38$ deg and $\beta_1 = 60$ deg.

where ϕ is any of the dependent variables (U, V, W, k, or ϵ), Γ the diffusion coefficient, and S_ϕ encompasses all remaining terms. The time-dependent terms are not included in Eq. (14) for the current steady flow problems. With the divergence theorem, Eq. (14) can be represented as follows for the arbitarily shaped control volume:

$$\int_A \rho \phi^{n+1} U_i n_i \mathrm{d}A = \int_A \frac{\Gamma_{\text{eff}}}{\sigma_\phi} \phi^{n+1}_{,i} n_i \mathrm{d}A + \int_R S_\phi \mathrm{d}R \tag{15}$$

where A is the boundary surface of the control volume R, and the superscript $n+1$ denotes the values at the $n+1$ iteration.

Various numerical experiments have indicated that current solution procedure, which is based on the primitive variables of the flow, converges rather slowly when applied to convection-dominated separated flows. To reduce oscillation of unknown variables during computation, the convection term in Eq. (14) is divided into explicit and implicit parts and Eq. (15) is rewritten as follows:

$$\frac{1}{2}\int_A \rho \phi^{n+1} U_i n_i \mathrm{d}A = \int_A \frac{\Gamma_{\text{eff}}}{\sigma_\phi} \phi^{n+1}_{,i} n_i \mathrm{d}A - \frac{1}{2}\int_A \rho \phi^n U_i n_i \mathrm{d}A + \int_R S_\phi \mathrm{d}R \tag{16}$$

where the convection term on the left-hand side is treated implicitly and the second term on the right-hand side is treated as a source term.

Various integrations in Eq. (16) are approximated by interpolating the values at nodal points of the computation grid. For the diffusion term in Eq. (16), central differencing is used. For the discretization of the convection term, various schemes have been proposed for stable and accurate solution.[12,13] The quadratic upwind interpolation scheme by Leonard[5] has been modified to get a stable solution for higher cell Reynolds numbers and has been used for the discretization of the convection term. The details of the modifications and numerical accuracy (third-order accurate in truncation error) are explained in an earlier report.[7]

The mean velocity, total energy, and turbulence quantities are solved simultaneously with the pressure field at the previous iteration. The pressure field is adjusted to satisfy the mass conservation. When finite difference equations for the mass and momentum conservation are not satisfied closely during iteration, strong coupling between pressure and velocity generates nonphysical oscillations and delays overall convergence. Issa's concept of the pressure implicit split operator[14] is extended further for nonorthogonal curvilinear coordinates. With the proposed concept, one more correction step is added at each iteration to get improved intermediate values for pressure and velocity fields. The intermediate values of velocity are first obtained with the pressure field of previous iterations

$$A_p \rho^n U_i^* = \Sigma A_{pm} U_{im}^* - \Delta_i p^n + S_i \tag{17}$$

where the asterisk denotes intermediate value at this step, A_p and A_{pm} are the finite difference coefficients, and n represents the value at the nth iteration. Since the values obtained with this equation do not satisfy mass conservation, corrective components of pressure and velocity are obtained by combining finite difference equations for pressure and velocity.

$$(\rho^* U_i^{**} - \rho^n U_i^*) = A_p^{-1} \Delta_i (p^* - p^n) \tag{18}$$

where U_i^{**} is the first corrected velocity component. Equation (18) is solved for p^* by taking the divergence of the equation and with the condition $\nabla \rho U_i^{**} = 0$. U_i^{**} and ρ^* are obtained with Eqs. (17) and (4).

In Eq. (18), the effect of convection [first term on the right-hand side of Eq. (17)] is neglected in order to facilitate the solution of this equation. An additional step is to include this convective effect in the intermediate solutions. With the values of *, **, and n,

$$\rho^{n+1}U_i^{n+1}-\rho^*U^{**}=A_p^{-1}\{\Sigma A_p^m(U_{im}^{**}-U_{im}^*)-\Delta_i(p^{n+1}-p^*)\} \tag{19}$$

The effect of convection is represented with the values of previous steps and is handled as a source term in solving Eq. (19). Again, the mass conservation condition for U_i^{n+1} is used to solve Eq. (19) and p^{n+1}, U^{n+1}, and ρ^{n+1} are obtained with Eqs. (19), (18), and (4). Various linear equations resulting from the current implicit scheme are solved by an iterative line-by-line procedure.

With the generalized curvilinear coordinates, unknown values at nine surrounding nodes (U_{im}) are used to update the unknown at the center of the control volume. Numerical experiments indicate that overall convergence rates diminish when off-diagonal terms are neglected.

Computational Grid

To represent the complex geometry of the compressor cascade (shown in Fig. 1) and distribute computational meshes in an optimum fashion, a nonorthogonal body-fitted grid is used. The grid is generated by solving a set of Poisson equations and mesh-point clustering is performed near the boundary with the method proposed by Sorenson and Steger.[15] Computational grids for the present study are given in Fig. 2, where two blade passages are shown to illustrate the grid distribution near the blade surface. The computational domain is one blade-to-blade passage. A fully staggered grid system is employed for the velocities and pressure to avoid decoupling effects between velocity and pressure that are frequently observed with the normal grid arrangement. On the computational domain, two velocity components are stored between the pressure nodes along the grid lines. Second-order forward or backward differences are used at the cells located on the blade surface and periodicity conditions are applied on the boundaries in the freestream. No special treatments have been performed for the control volumes at the leading and trailing edges. The inclined angles of the grid in the freestream are based on the flow attack angle β_1 and stagger angle.

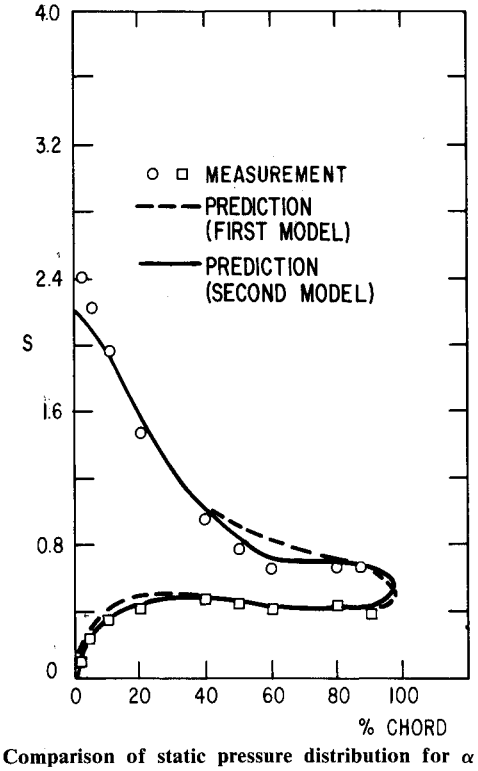

Fig. 4 Comparison of static pressure distribution for $\alpha=28$ deg and $\beta_1=60$ deg.

Boundary Conditions

The inlet boundary conditions were taken from the measurement where possible (U_i, k, and ϵ are specified). The value of turbulence kinetic energy at the inlet was maintained with the same experimental value. The rate of energy dissipation at the inlet section was assumed to be

$$\epsilon=C_\mu k^{3/2}/L \tag{20}$$

where L is the characteristic length scale and $L=0.01L_1$ (L_1 is the pitch of the cascade). At the exit, asymptotic boundary conditions (the second-order streamwise derivation of unknown variables is zero) are applied for unknown variables and the overall mass conservation is strictly imposed. The periodicity conditions are imposed on the corresponding nodes in the freestream for unknown variables and fluxes. At nodes nearest to the solid walls, the velocity vector is assumed to be on the plane parallel to the solid walls, and the wall function is applied for the velocity vector. With the assumption of local equilibrium and the wall function, the following relationships are obtained at the node next to the wall:

$$\tau_w=\frac{\rho C_\mu^{1/4}k_1^{1/2}U_1}{A\ell n(y_1C_\mu^{1/4}k_1^{1/2}/\nu)+B} \tag{21a}$$

$$\epsilon_1=A\frac{C_\mu^{1/4}k_1^{3/2}}{y_1} \tag{21b}$$

where $A=2.40$, $B=5.45$, and y_1 is the distance from the wall. The value of k_1 is estimated from the transport equation of the turbulence kinetic energy by neglecting the convective and diffusive effects through the wall. The first node is located 0.001 chord length away from the wall, and the node is located inside the inertial sublayer. ($y_1\sqrt{\tau_w}/\rho/\nu\sim 20$ at the trailing edge.) The fluctuations of the residual of the finite difference equations are monitored along with the total mass conservation. When these residuals, nondimensionalized with inlet flow quantities, are less than 10^{-4}, the solution is assumed to be converged. About 0.3 s is required per iteration of all unknowns on a CRAY-1 with 100×60 nodes and the final solution is obtained with 800 iterations with uniform distribution of unknown variables as the initial condition.

Comparison Between Numerical Prediction and Experimental Data

The experimental data of NACA 65-series compressor blades by Emery et al.[16] are used for comparison purposes. The experimental study includes a detailed survey of the static pressure distribution on the blade surface and section drag and lift coefficients, turning angle, etc., for various cascade settings of NACA 65-series airfoils. Numerical results for two different cascade settings of NACA 65-(18) 10 airfoils are presented. Some of the important parameters of the cascade settings are: chord length, 0.127 m; solidity, 1.5; inlet angle, 45 deg; and angles between flow direction and blade chord, 22 and 32 deg. The inlet velocity is 28.9 m/s and the Reynolds number based on the chord length is 245,000. Measured pressure distribution and section drag coefficient indicate that flow separation occurs for the second case (32 deg between flow direction and blade chord), while there is no flow separation for the first case.

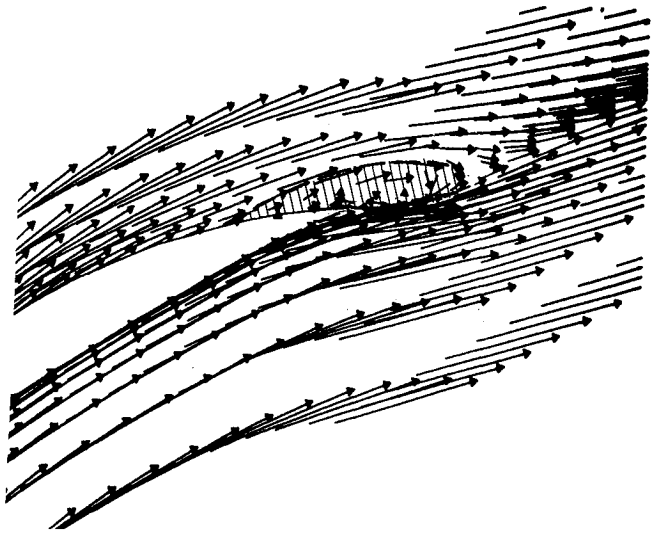

Fig. 5a Predicted mean velocity profiles near the trailing edge with the first model; $\alpha = 28$ deg, $\beta_1 = 60$ deg.

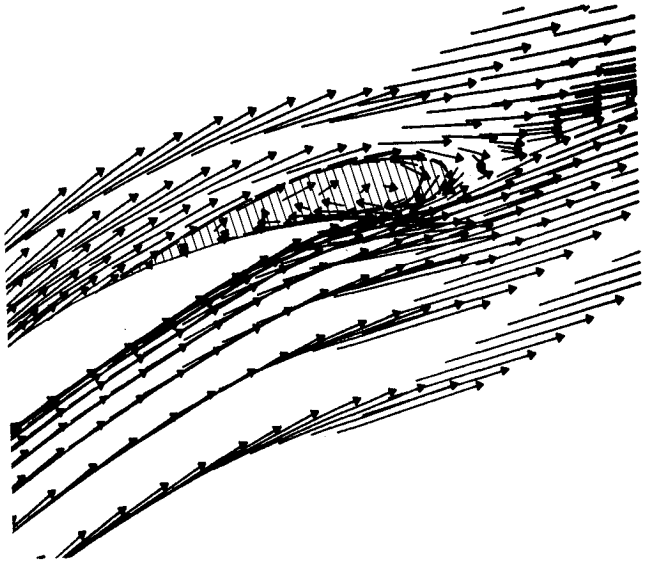

Fig. 5b Predicted mean velocity profiles near the trailing edge with the second model; $\alpha = 28$ deg, $\beta_1 = 60$ deg.

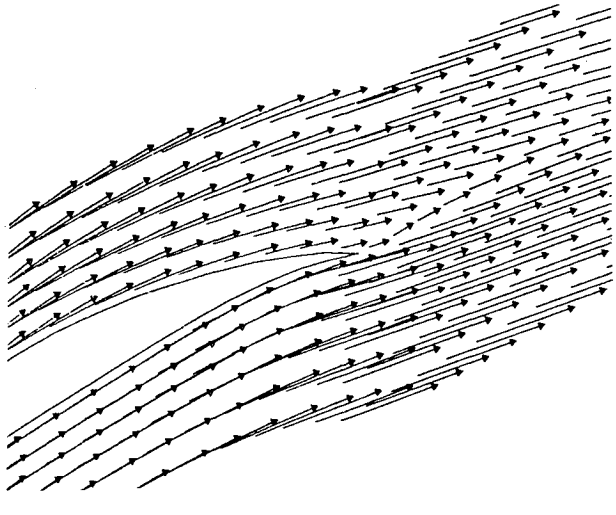

Fig. 5c Predicted mean velocity profiles near the trailing edge with coarse grid in the blade-to-blade direction.

Static Pressure Distribution

The static pressure distributions on the airfoil surface are compared in Figs. 3 and 4. All of the computations are made with the grid size of 100×60. For the lower incidence angle (22 deg), the flow is completely attached to the blade surface and the flow is primarily characterized as pressure-driven. Therefore, the pressure distributions with two different turbulence closure models are almost identical. Also good agreement for this unseparated flow case indicates that the grid size and other numerical procedures are adequate for the investigation of the current problems. In Fig. 4, the static pressure distributions with two different turbulence models are compared with the experimental data. The results with different turbulence closure schemes show some deviations near the trailing edge where the flow is separated. On the suction side of the airfoil, the local angular momentum increased with the radius of streamline curvature. Therefore, the effect of streamline curvature is to diminish turbulent diffusion and the flow separates earlier and the separation bubble becomes larger. As the separation bubble diminishes the effective area between the blade passage, significant change in static pressure distribution can be obtained depending on the size of the separated flow regime. As many earlier investigations have indicated,[6,7] the standard two-equation model does not represent the curvature effect correctly. With the two-equation model, a much higher value of turbulent diffusion is predicted near the trailing edge and the flow separation is delayed and the size of the separation bubble is underpredicted. The results in Fig. 4 show that the gross effect of streamline curvature is represented more adequately with the second model.

Mean Velocity

Since no detailed measurement of velocity around a cascade of airfoils at stall conditions has been reported, predicted velocity fields with different models are compared. The predicted mean velocity profiles for the higher incidence angle are compared in Fig. 5. As expected, a larger separation bubble is predicted with the second turbulence closure model. As expected, a smaller separated flow region is predicted due to numerical diffusion when an unrealistically smaller size of grid is used. With the same number of streamwise nodes, no flow separation is predicted when the blade-to-blade nodes are reduced more than one-half. The predicted velocity vector with 22 nodes in the normal direction is shown in Fig. 5c. Turbulence closure schemes based on simple mixing length or eddy viscosity are difficult to apply and predict unrealistic results for separated flow. Therefore, models simpler than two-equation models are not used for the current study.

Section Lift and Drag Coefficients and Turning Angle

Figure 6 shows the comparison for section lift and drag coefficients and turning angles for various incidence angles. All of the computations for different incidence angles were done with the same grid size (100×60). Two turbulence closure models predict very similar results for the low incidence angles. However, significant deviations are observed for off-design conditions. The section lift and drag coefficients are based on the following axial and tangential force coefficients:

$$C_{F,a} = \frac{F_a}{\frac{1}{2}\rho_1 W_1^2} b, \qquad C_{F,u} = \frac{F_u}{\frac{1}{2}\rho_1 W_1^2} b \tag{22}$$

where F_a and F_u are axial and tangential forces, respectively, W_1 the inlet total velocity, and b the chord of the airfoil.

The lift and drag coefficients are the components of these coefficients perpendicular and parallel, respectively, to the

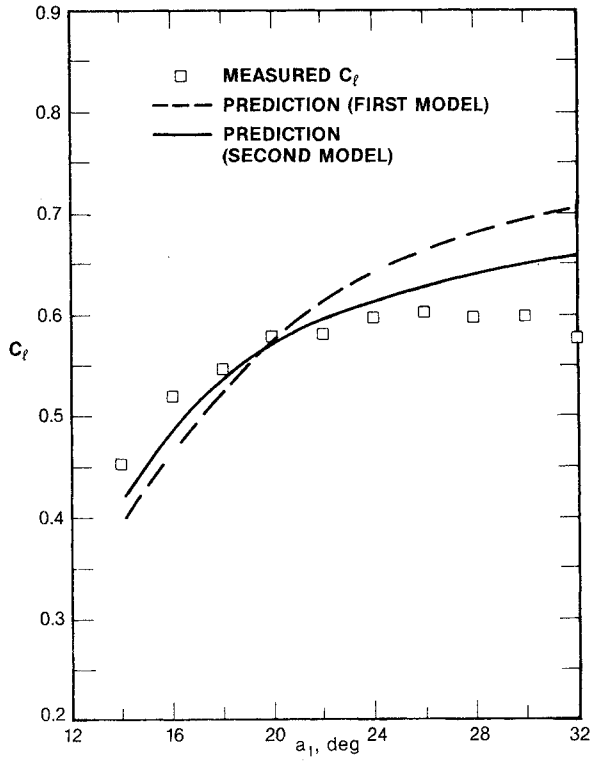

Fig. 6a Comparison of section lift coefficients.

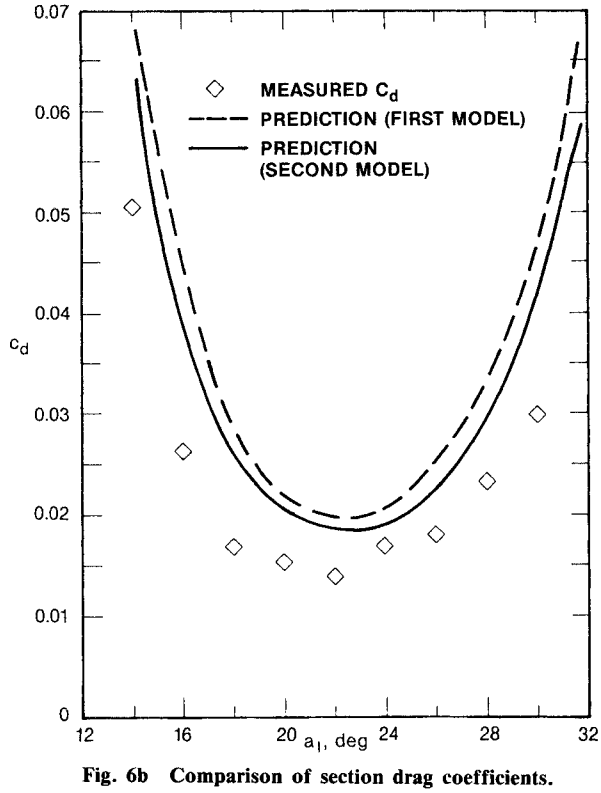

Fig. 6b Comparison of section drag coefficients.

vector mean velocity V_m, where V_m is the vectorial average of the velocities far upstream and far downstream. The axial and tangential forces in Eq. (18) were calculated with the flow condition far upstream and far downstream, as experimental values were estimated. At higher incidence angles, the numerical results show slight underturnings of the flow compared to the measurements. The drag coefficient is very sensitive to the W_m, which is also sensitive to the turning angle, and relatively large deviations between measured and computed values of drag coefficients can be obtained when

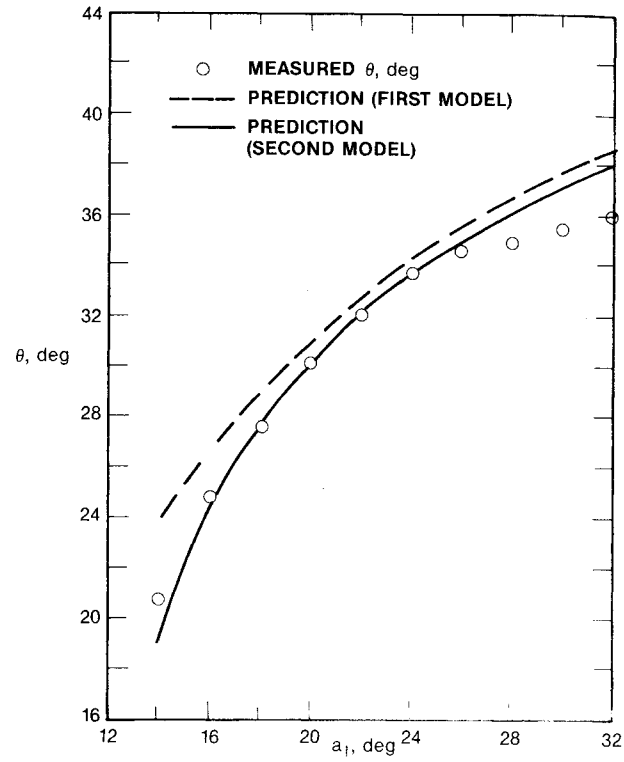

Fig. 6c Comparison of flow turning angles.

turning angles are not predicted exactly. However, the overall agreement for lift coefficient is reasonably good along with the turning angle itself. Here again, the second turbulence closure model predicts better than the first one, especially in the off-design regime.

Concluding Remarks

A numerical model is developed for the turbulent flowfields through a cascade of airfoils at stall conditions. Two different turbulence closure schemes (standard two-equation model and a curvature corrected algebraic Reynolds stress model) are tested and the results are compared. The following concluding remarks can be drawn from this study.

1) The developed numerical scheme with the turbulence closure scheme predicts complex static pressure distribution around a cascade of airfoils at stall conditions with accuracy satisfactory for most engineering practices.

2) For nonseparated flows, the flow is pressure-dominant and accurate predictions for static pressure distribution and turning angles are obtained with either turbulence scheme. For the flows at stall conditions, the size of the separated flow regime is rather sensitive to the used turbulence closure scheme and the second model predicted better results.

3) Although more detailed flow data, especially velocity measurements near the trailing edge, are necessary for comprehensive evaluation and further development of the model, the presently developed model can be used to study various flow characteristics at stall conditions and the off-design performance of cascades of airfoils.

References

[1]Steger, J. L., Pullman, T. H., and Chima, R. V., "An Implicit Finite Difference Code for Inviscid and Viscous Cascade Flow," AIAA Paper 80-1427, 1980.

[2]Shamroth, S., Gibeling, H. J., and McDonald, H., "A Navier-Stokes Solution for Laminar and Turbulent Flow Through a Cascade of Airfoils," AIAA Paper 80-1426, 1980.

[3]Dodge, R. P., "Numerical Method for Two-Dimensional and Three-Dimensional Viscous Flows," AIAA Paper 76-425, July 1976.

[4]McNally, W. D. and Sockol, P. M., "Computational Methods for Internal Flows with Emphasis on Turbomachinery," NASA TM X-2764, 1981.

[5]Leonard, B. P., "A Stable and Accurate Convective Modeling Procedure Based on Quadratic Upstream Interpolation," *Computer Methods in Applied Mechanics and Engineering*, Vol. 19, 1979, pp. 59-98.

[6]Leschziner, M. A. and Rodi, W., "Calculation of Annular and Twin Parallel Jets Using Various Discretization Schemes and Turbulence Model Variations," *Transactions of ASME, Journal of Fluids Engineering*, June 1981, pp. 352-360.

[7]Hah, C., "Calculation of Planar, Conical and Annular Diffuser Flows with Inlet Swirl and Inlet Distortion Effects," *AIAA Journal*, Vol. 21, Aug. 1983, pp. 1127-1133.

[8]Rodi, W., "Turbulence Models and Their Application in Hydraulics," State-of-the-Art Paper, June 1980.

[9]Hah, C., "Three-Dimensional Structure and Turbulence Closure of the Wake Developing in a Wall Shear Layer," *AIAA Journal*, Vol. 20, Nov. 1982, pp. 1599-1605.

[10]Bradshaw, P., "Effects of Streamline Curvature on Turbulent Flow," AGARDOgraph 169, 1973.

[11]Hah, C. and Lakshminarayana, B., "Prediction of Two- and Three-Dimensional Asymmetric Turbulent Wakes, Including Curvature and Rotation Effects," *AIAA Journal*, Vol. 18, Oct. 1980, pp. 1196-1204.

[12]Raithby, G. D., "Skew-Upwind Differencing Schemes for Problems Involving Fluid Flow," *Computer Methods in Applied Mechanics and Engineering*, Vol. 9, 1976, pp. 153-164.

[13]Leschziner, M. A., "Practical Evaluation of Three Finite-Difference Schemes for the Computation of Steady State Recirculating Flows," *Computer Methods in Applied Mechanics and Engineering*, Vol. 23, 1980, pp. 293-312.

[14]Issa, R. I., "Solution of Implicitly Discretized Fluid Flow Equations by Operator-Splitting," Department of Mineral Resources Engineering, Imperial College, London, Internal Report, 1982.

[15]Sorenson, R. L. and Steger, J. L., "Numerical Generation of Two-Dimensional Grids by the Use of Poisson's Equations with Grid Control at Boundaries," *Proceedings of Workshop on Numerical Grid Generation,* NASA Langley Research Center, Hampton, Va., Oct. 1980.

[16]Emery, J. C., Herrig, L. J., Erwin, J. R., and Felix, A. R., "Systematic Two-Dimensional Cascade Tests of NACA 65-Series Compressor Blades at Low Speeds," NACA 1368, 1958.